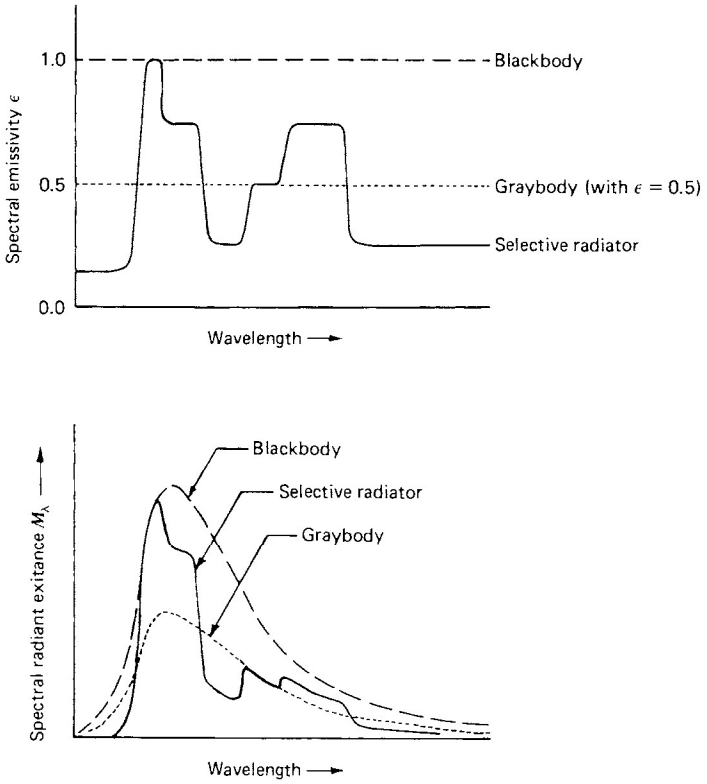

Figure 5.13 Spectral emissivities and radiant exitances for a blackbody, a graybody, and a selective radiator. (Adapted from Hudson, 1969.)

Many materials radiate like blackbodies over certain wavelength intervals. For example, as shown in Figure 5.14*a*, water is very close (ε is 0.98 to 0.99) to behaving as a blackbody radiator in the 6- to 14-μm range. Other materials, such as quartz, act as a selective radiator, with considerable variation in emissivity at different wavelengths in the 6- to 14-μm range (Figure 5.14*b*).

The 8- to 14-μm region of spectral radiant exitance is of particular interest since it not only includes an atmospheric window but also contains the peak energy emissions for most surface features. That is, the ambient temperature of earth surface features is normally about 300 K, at which temperature the peak emissions will occur at approximately 9.7 μm. For these reasons, most thermal sensing is performed in the 8- to 14-μm region of the spectrum. The emissivities of different objects vary greatly with material type in this range. However, for any given material type, emissivity is often considered constant in the 8- to 14-μm range when broadband sensors are being used. This means that within this spectral region materials are often treated as graybodies. However, close examination of emissivity versus wavelength for

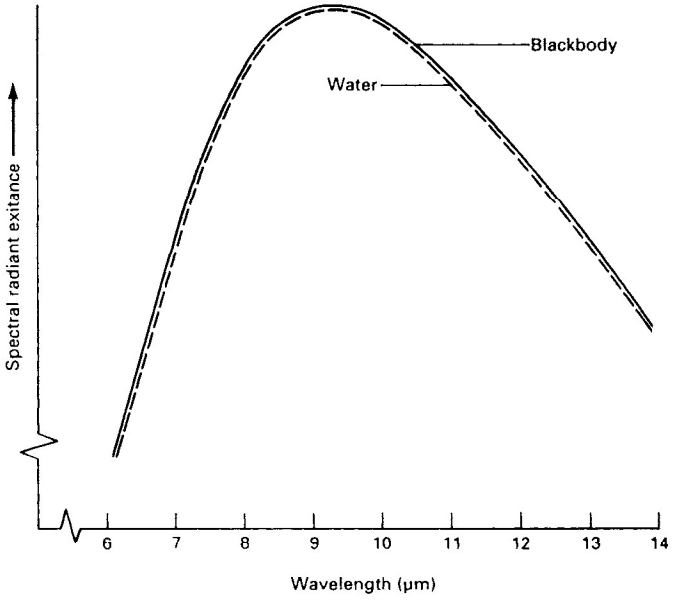

(a)

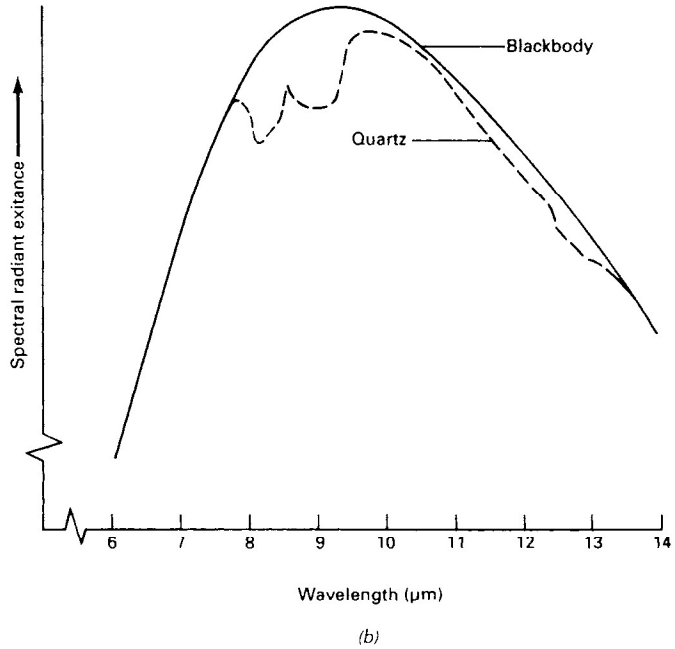

(b)

Figure 5.14 Comparison of spectral radiant exitances for (*a*) water versus a blackbody and (*b*) quartz versus a blackbody. (For additional curves, see Salisbury and D'Aria, 1992.)

materials in this wavelength range shows that values can vary considerably with wavelength. Therefore, the within-band emissivities of materials sensed in the 10.5- to 11.5-μm range [National Oceanic and Atmospheric Administration (NOAA) AVHRR band 4] would not necessarily be the same as the within-band emissivities of materials sensed in the 10.4- to 12.5-μm range (Landsat TM band 6). Furthermore, emissivities of materials vary with material condition. A soil that has an emissivity of 0.92 when dry could have an emissivity of 0.95 when wet (water-coated soil particles have an emissivity approaching that of water). Objects such as deciduous tree leaves can have a dif-

TABLE 5.2 Typical Emissivities of Various Common Materials over the Range of 8–14 μm

Material	Typical Average Emissivity ε over 8–14 μm[a]
Clear water	0.98–0.99
Wet snow	0.98–0.99
Human skin	0.97–0.99
Rough ice	0.97–0.98
Healthy green vegetation	0.96–0.99
Wet soil	0.95–0.98
Asphaltic concrete	0.94–0.97
Brick	0.93–0.94
Wood	0.93–0.94
Basaltic rock	0.92–0.96
Dry mineral soil	0.92–0.94
Portland cement concrete	0.92–0.94
Paint	0.90–0.96
Dry vegetation	0.88–0.94
Dry snow	0.85–0.90
Granitic rock	0.83–0.87
Glass	0.77–0.81
Sheet iron (rusted)	0.63–0.70
Polished metals	0.16–0.21
Aluminum foil	0.03–0.07
Highly polished gold	0.02–0.03

[a]Emissivity values (ordered from high to low) are typical average values for the materials listed over the range of 8–14 μm. Emissivities associated with only a portion of the 8–14-μm range can vary significantly from these values. Furthermore, emissivities for the materials listed can vary significantly, depending on the condition and arrangement of the materials (e.g., loose soil vs. compacted soil, individual tree leaves vs. tree crowns).

ferent emissivity when a single leaf is sensed (0.96) than when an entire tree crown is sensed (0.98). Table 5.2 indicates some typical values of emissivity over the 8- to 14-μm-wavelength range for various common materials.

It should be noted that as objects are heated above ambient temperature, their emissive radiation peaks shift to shorter wavelengths. In special-purpose applications, such as forest fire mapping, systems operating in the 3- to 5-μm atmospheric window may be used. These systems offer improved definition of hot objects at the expense of the surrounding terrain at ambient temperature.

Atmospheric Effects

As is the case with all passive remote sensing systems, the atmosphere has a significant effect on the intensity and spectral composition of the energy recorded by a thermal system. As mentioned, atmospheric windows (Figure 5.15) influence the selection of the optimum spectral bands within which to measure thermal energy signals. Within a given window, the atmosphere intervening between a thermal sensor and the ground can increase or decrease the apparent level of radiation coming from the ground. The effect that the atmosphere has on a ground signal will depend on the degree of atmospheric absorption, scatter, and emission at the time and place of sensing.

Gases and suspended particles in the atmosphere may absorb radiation emitted from ground objects, resulting in a decrease in the energy reaching a

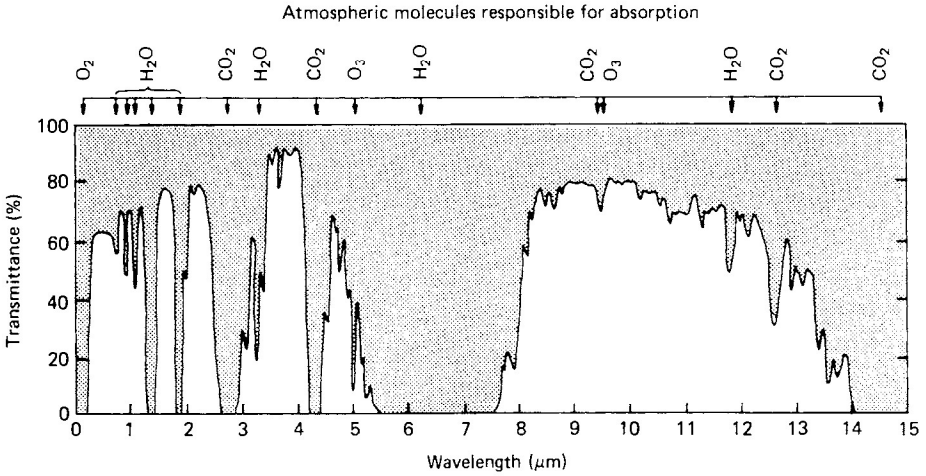

Figure 5.15 Atmospheric absorption of the wavelength range 0 to 15 μm. Note the presence of atmospheric windows in the thermal wavelength regions 3 to 5 μm and 8 to 14 μm. (Adapted from Hudson, 1969.)

thermal sensor. Ground signals can also be attenuated by scattering in the presence of suspended particles. On the other hand, gases and suspended particles in the atmosphere may emit radiation of their own, adding to the radiation sensed. Hence, atmospheric absorption and scattering tend to make the signals from ground objects appear colder than they are, and atmospheric emission tends to make ground objects appear warmer than they are. Depending on atmospheric conditions during imaging, one of these effects will outweigh the other. This will result in a biased sensor output. Both effects are directly related to the atmospheric path length, or distance, through which the radiation is sensed.

Thermal sensor measurements of temperature can be biased by as much as 2°C or more when acquired at altitudes as low as 300 m. Of course, meteorological conditions have a strong influence on the form and magnitude of the thermal atmospheric effects. Fog and clouds are essentially opaque to thermal radiation. Even on a clear day, aerosols can cause major modifications of signals sensed. Dust, carbon particles, smoke, and water droplets can all modify thermal measurements. These atmospheric constituents vary with site, altitude, time, and local weather conditions.

Atmospheric effects on radiant temperature measurements usually may not be ignored. The various strategies commonly employed to compensate for atmospheric effects are described later in this chapter. We now consider how thermal radiation interacts with ground objects.

Interaction of Thermal Radiation with Terrain Elements

In thermal sensing we are interested in the radiation emitted from terrain features. However, the energy radiated *from* an object usually is the result of energy incident *on* the feature. In Section 1.4 we introduced the basic notion that energy incident on the surface of a terrain element can be absorbed, reflected, or transmitted. In accordance with the principle of conservation of energy, we can state the relationship between incident energy and its disposition upon interaction with a terrain element as

$$E_I = E_A + E_R + E_T \tag{5.5}$$

where

E_I = energy incident on surface of terrain element
E_A = component of incident energy absorbed by terrain element
E_R = component of incident energy reflected by terrain element
E_T = component of incident energy transmitted by terrain element

If Eq. 5.5 is divided by the quantity E_I, we obtain the relationship

$$\frac{E_I}{E_I} = \frac{E_A}{E_I} + \frac{E_R}{E_I} + \frac{E_T}{E_I} \tag{5.6}$$

The terms on the right side of Eq. 5.6 comprise ratios that are convenient in further describing the nature of thermal energy interactions. We define

$$\alpha(\lambda) = \frac{E_A}{E_I} \quad \rho(\lambda) = \frac{E_R}{E_I} \quad \tau(\lambda) = \frac{E_T}{E_I} \tag{5.7}$$

where

$\alpha(\lambda)$ = *absorptance* of terrain element
$\rho(\lambda)$ = *reflectance* of terrain element
$\tau(\lambda)$ = *transmittance* of terrain element

We can now restate Eq. 5.5 in the form

$$\alpha(\lambda) + \rho(\lambda) + \tau(\lambda) = 1 \tag{5.8}$$

which defines the interrelationship among a terrain element's absorbing, reflecting, and transmitting properties.

Another ingredient necessary is the *Kirchhoff radiation law*. It states that the spectral emissivity of an object equals its spectral absorptance:

$$\varepsilon(\lambda) = \alpha(\lambda) \tag{5.9}$$

Paraphrased, "good absorbers are good emitters." While Kirchhoff's law is based on conditions of thermal equilibrium, the relationship holds true for most sensing conditions. Hence, if we apply it in Eq. 5.8, we may replace $\alpha(\lambda)$ with $\varepsilon(\lambda)$, resulting in

$$\varepsilon(\lambda) + \rho(\lambda) + \tau(\lambda) = 1 \tag{5.10}$$

Finally, in most remote sensing applications the objects we deal with are assumed to be opaque to thermal radiation. That is, $\tau(\lambda) = 0$, and it is therefore dropped from Eq. 5.10 such that

$$\varepsilon(\lambda) + \rho(\lambda) = 1 \tag{5.11}$$

Equation 5.11 demonstrates the direct relationship between an object's emissivity and its reflectance in the thermal region of the spectrum. The lower an object's reflectance, the higher its emissivity. The higher an object's reflectance, the lower its emissivity. For example, water has nearly negligible reflectance in the thermal spectrum. Therefore, its emissivity is essentially 1. In contrast, a material such as sheet metal is highly reflective of thermal energy, so it has an emissivity much less than 1.

The emissivity of an object has an important implication when measuring radiant temperatures. Recall that the Stefan–Boltzmann law, as stated in Eq. 5.3 ($M = \sigma T^4$), applied to blackbody radiators. We can extend the blackbody radiation principles to real materials by reducing the radiant exitance M by the emissivity factor ε such that

$$M = \varepsilon \sigma T^4 \tag{5.12}$$

TABLE 5.3 Kinetic versus Radiant Temperature for Four Typical Material Types

		Kinetic Temperature T_{kin}		Radiant Temperature $T_{rad} = \varepsilon^{1/4} T_{kin}$	
Object	Emissivity ε	K	°C	K	°C
Blackbody	1.00	300	27	300.0	27.0
Vegetation	0.98	300	27	298.5	25.5
Wet soil	0.95	300	27	296.2	23.2
Dry soil	0.92	300	27	293.8	20.8

Equation 5.12 describes the interrelationship between the measured signal a thermal sensor "sees," M, and the parameters of temperature and emissivity. Note that because of emissivity differences, earth surface features can have the same temperature and yet have completely different radiant exitances.

The output from a thermal sensor is a measurement of the radiant temperature of an object, T_{rad}. Often, the user is interested in relating the radiant temperature of an object to its kinetic temperature, T_{kin}. If a sensor were to view a blackbody, T_{rad} would equal T_{kin}. For all real objects, however, we must account for the emissivity factor. Hence, the kinetic temperature of an object is related to its radiant temperature by

$$T_{rad} = \varepsilon^{1/4} T_{kin} \tag{5.13}$$

Equation 5.13 expresses the fact that for any given object the radiant temperature recorded by a remote sensor will always be less than the kinetic temperature of the object. This effect is illustrated in Table 5.3, which shows the kinetic versus the radiant temperatures for four objects having the same kinetic temperature but different emissivities. Note how kinetic temperatures are always underestimated if emissivity effects are not accounted for in analyzing thermal sensing data.

A final point to be made here is that *thermal sensors detect radiation from the surface (approximately the first 50 μm) of ground objects*. This radiation may or may not be indicative of the internal bulk temperature of an object. For example, on a day of low humidity, a water body having a high temperature will manifest evaporative cooling effects at its surface. Although the bulk temperature of the water body could be substantially warmer than that of its surface temperature, a thermal sensor would record only the surface temperature.

5.8 INTERPRETING THERMAL SCANNER IMAGERY

Successful interpretations of thermal imagery have been made in many fields of application. These include such diverse tasks as determining rock type and

structure, locating geologic faults, mapping soil type and soil moisture, locating irrigation canal leaks, determining the thermal characteristics of volcanoes, studying evapotranspiration from vegetation, locating cold-water springs, locating hot springs and geysers, determining the extent and characteristics of thermal plumes in lakes and rivers, studying the natural circulation patterns in water bodies, determining the extent of active forest fires, and locating subsurface fires in landfills or coal refuse piles.

Most thermal scanning operations, such as geologic and soil mapping, are qualitative in nature. In these cases, it is not usually necessary to know absolute ground temperatures and emissivities, but simply to study relative differences in the radiant temperatures within a scene. However, some thermal scanning operations require quantitative data analysis in order to determine absolute temperatures. An example would be the use of thermal scanning as an enforcement tool by a state department of natural resources to monitor surface water temperatures of the effluent from a nuclear power plant.

Various times of day can be utilized in thermal scanning studies. Many factors influence the selection of an optimum time or times for acquiring thermal data. Mission planning and image interpretation must take into consideration the effects of diurnal temperature variation. The importance of diurnal effects is shown in Figure 5.16, which illustrates the relative radiant temperatures of soils and rocks versus water during a typical 24-hr period.

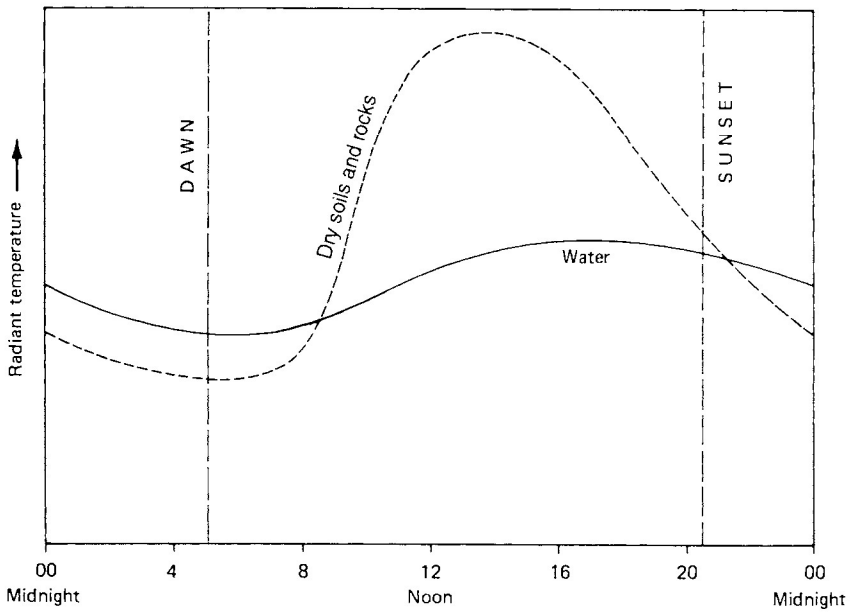

Figure 5.16 Generalized diurnal radiant temperature variations for soils and rocks versus water.

Note that just before dawn a quasi-equilibrium condition is reached where the slopes of the temperature curves for these materials are very small. After dawn, this equilibrium is upset and the materials warm up to a peak that is reached sometime after noon. Maximum scene contrast normally occurs at about this time and cooling takes place thereafter.

Temperature extremes and heating and cooling rates can often furnish significant information about the type and condition of an object. Note, for example, the temperature curve for water. It is distinctive for two reasons. First, its range of temperature is quite small compared to that of soils and rocks. Second, it reaches its maximum temperature an hour or two after the other materials. As a result, terrain temperatures are normally higher than water temperatures during the day and lower during the night. Shortly after dawn and near sunset, the curves for water and the other features intersect. These points are called thermal *crossovers* and indicate times at which no radiant temperature difference exists between two materials.

The extremes and rates of temperature variation of any earth surface material are determined, among other things, by the material's thermal conductivity, capacity, and inertia. *Thermal conductivity* is a measure of the rate at which heat passes through a material. For example, heat passes through metals much faster than through rocks. *Thermal capacity* determines how well a material stores heat. Water has a very high thermal capacity compared to other material types. *Thermal inertia* is a measure of the response of a material to temperature changes. It increases with an increase in material conductivity, capacity, and density. In general, materials with high thermal inertia have more uniform surface temperatures throughout the day and night than materials of low thermal inertia.

During the daytime, direct sunlight differentially heats objects according to their thermal characteristics and their sunlight absorption, principally in the visible and near-IR portion of the spectrum. Reflected sunlight can be significant in imagery utilizing the 3- to 5-μm band. Although reflected sunlight has virtually no direct effect on imagery utilizing the 8- to 14-μm band, daytime imagery contains thermal "shadows" in cool areas shaded from direct sunlight by objects such as trees, buildings, and some topographic features. Also, slopes receive differential heating according to their orientation. In the Northern Hemisphere, south-facing slopes receive more solar heating than north-facing slopes. Many geologists prefer "predawn" imagery for their work as this time of day provides the longest period of reasonably stable temperatures, and "shadow" effects and slope orientation effects are minimized. However, aircraft navigation over areas selected for thermal image acquisition is more difficult during periods of darkness, when ground features cannot be readily seen by the pilot. Other logistics also enter into the timing of thermal scanning missions. For example, scanning of effluents from power plant operations normally must be conducted during periods of peak power generation.

A number of thermal images are illustrated in the remainder of this chapter. In all cases, darker image tones represent cooler radiant temperatures and lighter image tones represent warmer radiant temperatures. This is the representation most commonly used in thermal images of earth surface features. In meteorological applications, the reverse representation is used to preserve the light-toned appearance of clouds.

Figure 5.17 illustrates the contrast between daytime (*a*) and nighttime (*b*) thermal images. The water in this scene (note the large lake at right and the small, lobed pond in lower center) appears cooler (darker) than its surroundings during the daytime and warmer (lighter) at night. The kinetic water temperature has changed little during the few hours of elapsed time between these images. However, the surrounding land areas have cooled considerably during the evening hours. Again, water normally appears cooler than its surroundings on daytime thermal images and warmer on nighttime thermal images, except for the case of open water surrounded by frozen or snow-covered ground where the water would appear warmer day and night. Trees can be seen many places in these images (note the area above and to the right of the small pond). Trees generally appear cooler than their surroundings during the daytime and warmer at night. Tree shadows appear in many places in the daytime image (note the residential area at upper left) but are not noticeable in the nighttime image. Paved areas (streets and parking lots) appear relatively warm both day and night. The pavement surfaces heat up to temperatures higher than their surroundings during the daytime and lose heat relatively slowly at night, thus retaining a temperature higher than their surroundings.

Figure 5.18 is a daytime thermal image showing the former shoreline of glacial Lake Middleton, an ephemeral glacial lake that is now primarily agricultural fields. This was a small lake, about 800 ha in extent at its maximum. At its lowest level, the lake was only about 80 ha in size. The beach ridge associated with this lowest lake level is shown at B. The ridge is most evident at the lower right because the prevailing winds at the time of its formation were from the upper left. The ridge is a small feature, only 60 m wide and $\frac{1}{2}$ to 1 m higher than the surrounding lakebed material. The beach ridge has a fine sandy loam surface soil 0.3 to 0.45 m thick underlain by deep sandy materials. The lakebed soils (A) are silt loam to a depth of at least 1.5 m and are seasonally wet with a groundwater table within 0.6 m of the ground surface in the early spring. At the time of this thermal image, most of the area shown here was covered with agricultural crops. The scanner sensed the radiant temperature of the vegetation over the soils rather than the bare soils themselves. Based on field radiometric measurements, the radiant temperature of the vegetation on the dry, sandy beach ridge soil is 16°C, whereas that over the wetter, siltier lakebed soil is 13°C. Although prominent on this thermal image, the beach ridge is often overlooked on panchromatic aerial photographs and is only partially mapped on a soil map of the area. Also seen on

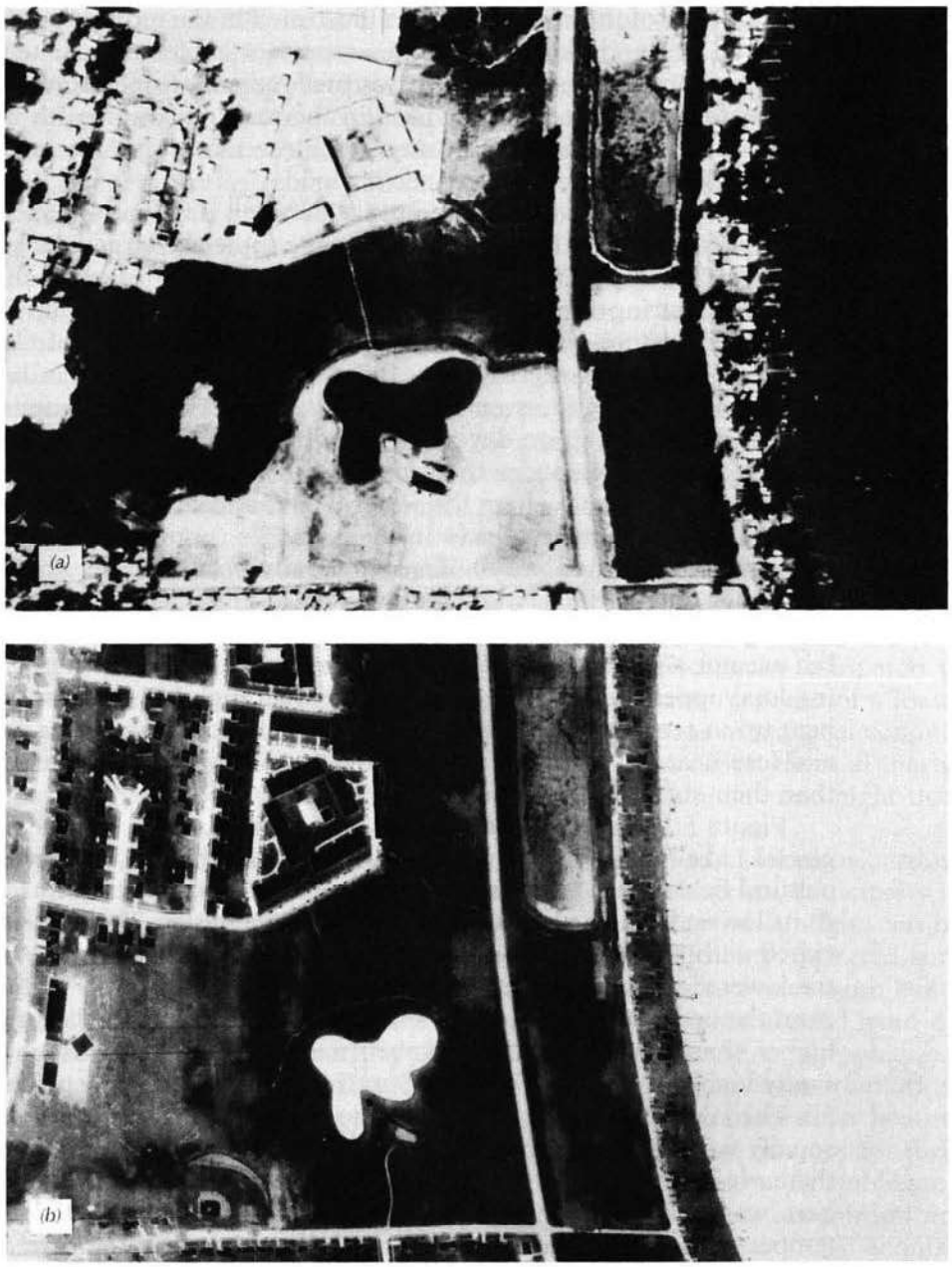

Figure 5.17 Daytime and nighttime thermal images, Middleton, WI: (*a*) 2:40 P.M., (*b*) 9:50 P.M.; 600 m flying height, 5 mrad IFOV. (Courtesy National Center for Atmospheric Research.)

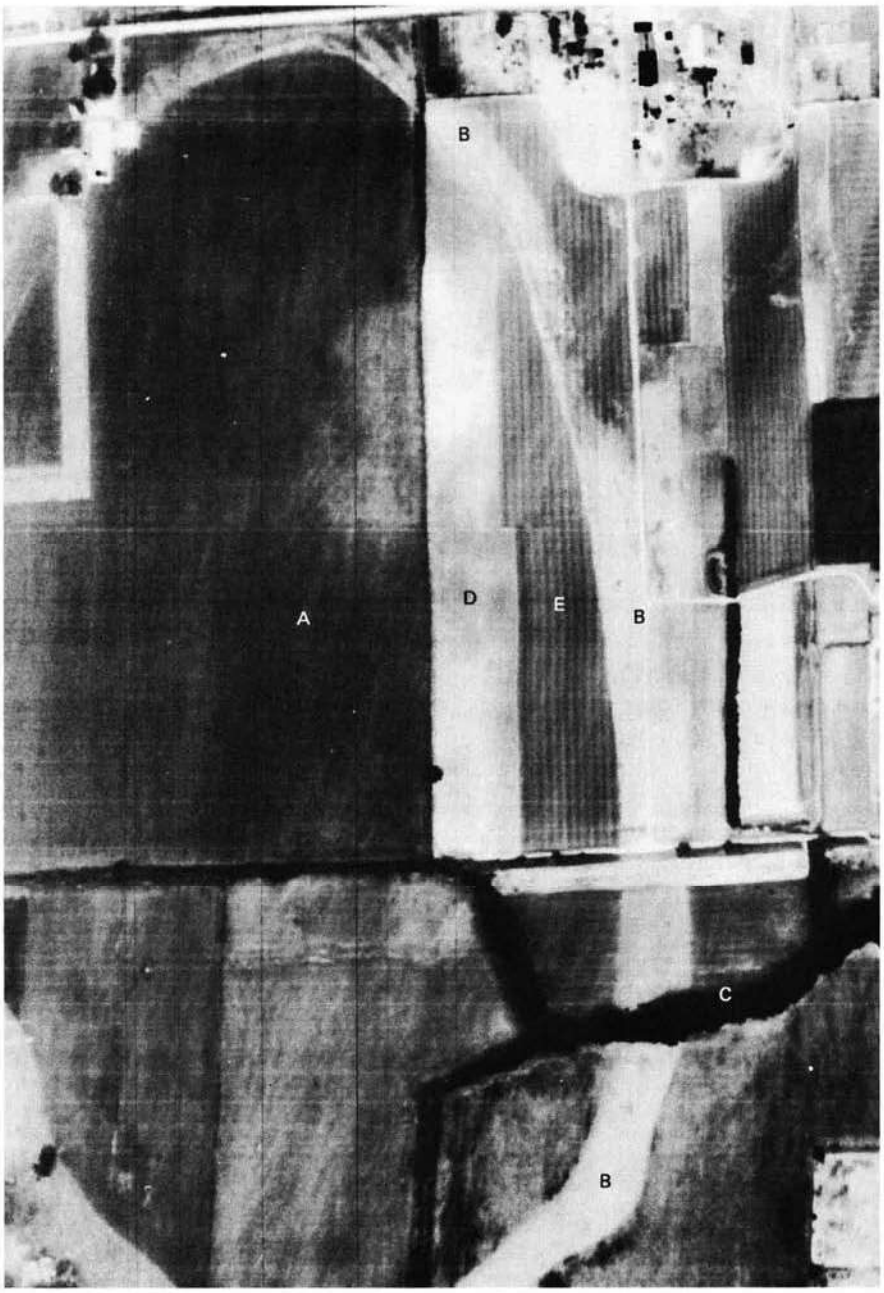

Figure 5.18 Daytime thermal image. Middleton, WI, 9:40 A.M., 600 m flying height, 5 mrad IFOV. (Courtesy National Center for Atmospheric Research.)

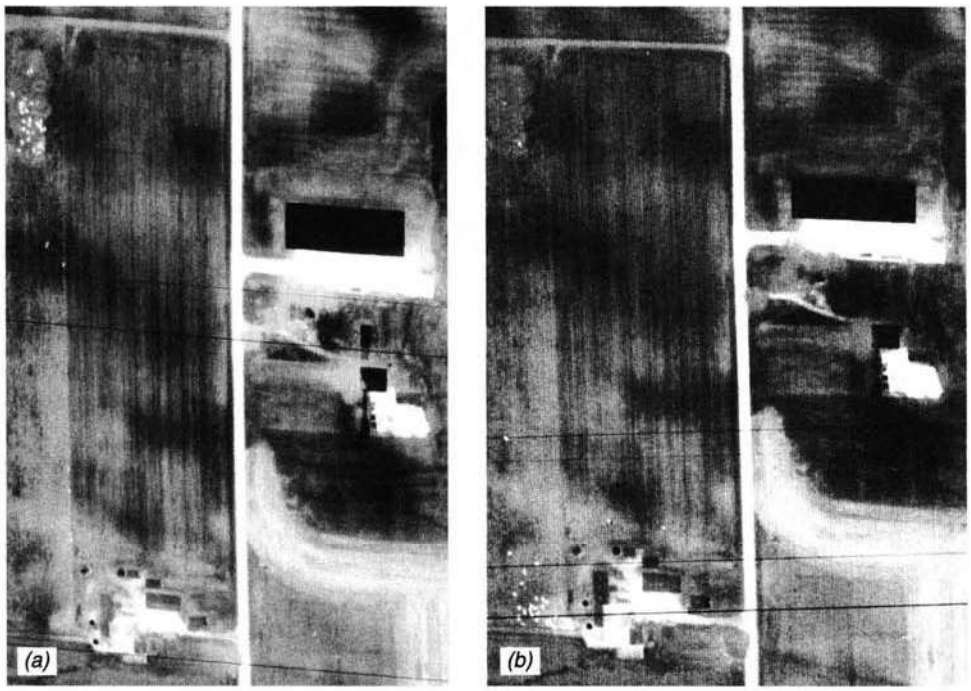

Figure 5.19 Nighttime thermal images, Middleton, WI: (*a*) 9:50 P.M., (*b*) 1:45 A.M.; 600 m flying height, 5 mrad IFOV. (Courtesy National Center for Atmospheric Research.)

this thermal image are trees at C, bare soil at D, and closely mowed grass (a sod farm) at E.

Figure 5.19 contains two nighttime thermal images illustrating the detectability of relatively small features on large-scale imagery. In Figure 5.19*a* (9:50 P.M.), a group of 28 cows can be seen as white spots near the upper left. In Figure 5.19*b* (1:45 A.M.), they have moved near the bottom of the image. (Deer located in flat areas relatively free of obstructing vegetation have also been detected, with mixed success, on thermal imagery.) The large, rectangular, very dark-toned object near the upper right of Figure 5.19*a* is a storage building with a sheet metal roof having a low emissivity. Although the kinetic temperature of the roof may be as warm as or warmer than the surrounding ground, its radiant temperature is low due to its low emissivity.

Figure 5.20 illustrates thermal imagery acquired with a high resolution scanner system. The image was acquired using a 0.25-mrad IFOV. The corresponding ground resolution cell size is approximately 0.3 m. This enlargement illustrates the spatial detail observable in the imagery. For example, several helicopters parked near hangers can be clearly seen in the enlarged image. Note also the "thermal shadow" left by two helicopters that are not in

Figure 5.20 Daytime thermal image, Quantico, VA, 0.25 mrad IFOV. (Courtesy RECON/OPTICAL, Inc.)

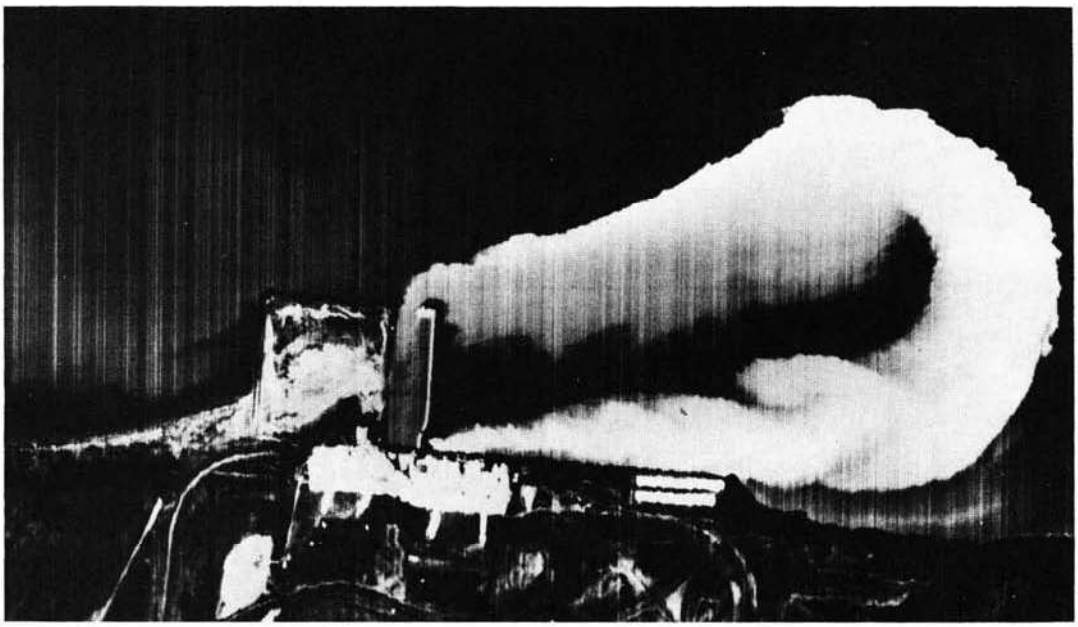

Figure 5.21 Daytime thermal image, Oak Creek Power Plant, WI, 1:50 P.M., 800 m flying height, 2.5 mrad IFOV. (Courtesy Wisconsin Department of Natural Resources.)

their original parked positions. Two helicopters can also be seen with their blades running while sitting on the helipad in the lower right.

Figure 5.21 illustrates the heated cooling water from a coal-fired power plant discharging into Lake Michigan. This daytime thermal image shows that the plant's cooling system is recirculating its heated discharge water. Heated water initially flows to the right. Winds from the upper right at 5 m/sec cause the plume to double back on itself, eventually flowing into the intake channel. The ambient lake temperature is about 4°C. The surface water temperatures in the plume are 11°C near the submerged discharge and 6°C in the intake channel. On a late winter day with cold lake temperatures, such as shown here, the recirculating plume does not cause problems with the power plant operation. However, such an event could cause operational problems during the summer because the intake water would be warmer than acceptable for the cooling system.

The use of aerial thermal scanning to study heat loss from buildings has been investigated in many cities. Figure 5.22 illustrates the typical form of imagery acquired in such studies. Note the striking differences among the radiant temperatures of various roofs as well as the temperature differences between various house roofs and garage/carport roofs of the same house. Such images are often useful in assessing inadequate or damaged insulation and roofing materials. The dark-toned streaks aligned from upper right to lower

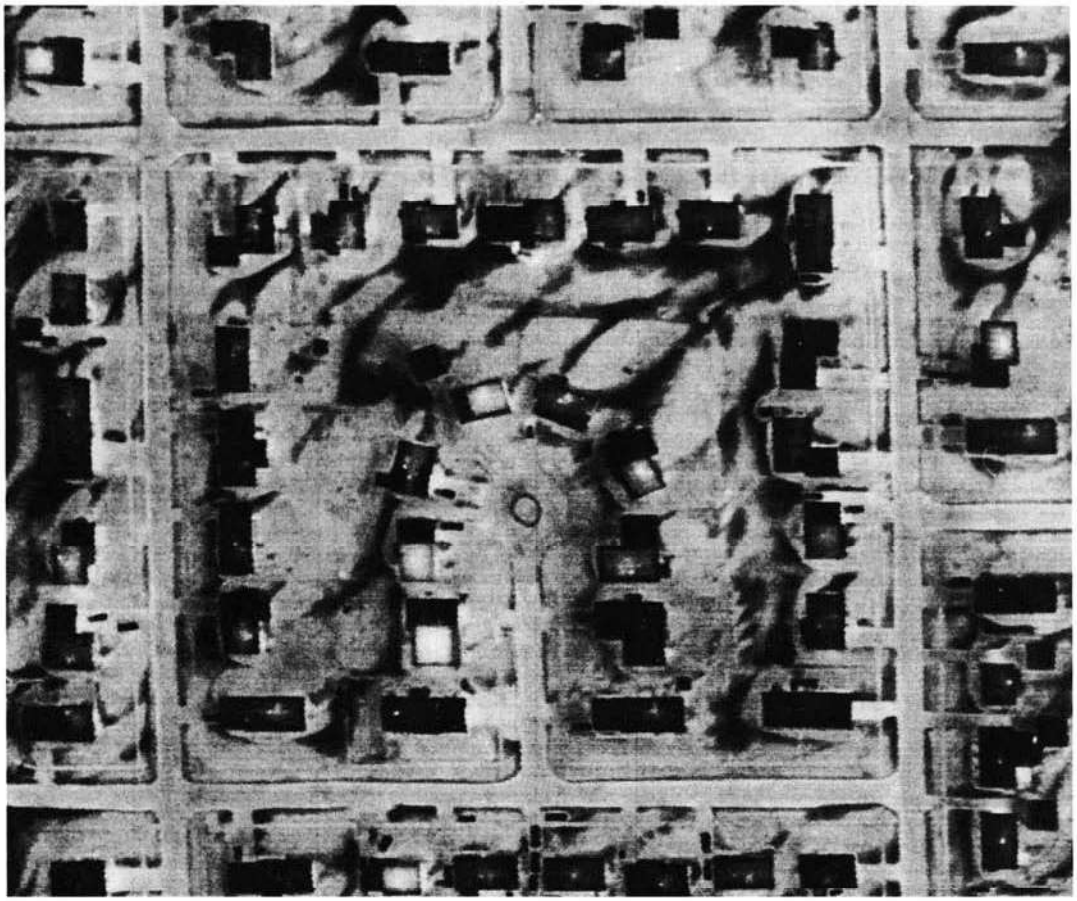

Figure 5.22 Nighttime thermal image depicting building heat loss in an Iowa City, approximately 2:00 A.M., snow-covered ground, air temperature approximately −4°C, 460 m flying height, 1 mrad IFOV. (Courtesy Iowa Utility Association.)

left on the ground areas between houses result from the effects of wind on the snow-covered ground.

Although aerial thermal scanning can be used to estimate the amount of energy radiated from the roofs of buildings, *the emissivity of the roof surfaces must be known to determine the kinetic temperature of the roof surfaces*. With the exception of unpainted sheet metal roofs (Figure 5.19), which have a very low emissivity, roof emissivities vary from 0.88 to 0.94. (Painted metal surfaces assume the emissivity characteristics of the particular paint used.)

Thermal scanning of roofs to estimate heat loss is best accomplished on cold winter nights at least 6 to 8 hr after sunset, in order to minimize the effects of solar heating. Alternatively, surveys can be conducted on cold overcast winter days. In any case, roofs should be neither snow covered nor wet. Because of

the side-looking characteristics of scanner images, the scanner vertically views the roof tops of buildings only directly beneath the plane. At the edge of the scan, it views the rooftops plus a portion of building sides. Roof pitch affects the temperature of roofs. A flat roof directly faces a night sky that is 20 to 30°C cooler than ambient air temperature and will therefore lose heat by radiation. Sloping roofs often receive radiation from surrounding buildings and trees, keeping their surfaces warmer than flat roofs. Attic ventilation characteristics must also be taken into account when analyzing roof heat loss.

When mapping heat loss by aerial thermal scanning, it must also be realized that heat loss from roofs constitutes only a portion of the heat lost from buildings, as heat is also lost through walls, doors, windows, and foundations. It is estimated that a house with comparable insulation levels in all areas loses about 10 to 15 percent of its heat through the roof. Homes with well-insulated walls and poorly insulated ceilings may lose more heat through the roof.

An alternative and supplement to aerial thermal scanning is the use of ground-based thermal scanning systems. Applications of these imaging systems range from detecting faulty electrical equipment (such as overheated transformers) to monitoring industrial processes to medical diagnosis. Depending on the detector used, the systems operate in the 3- to 5-μm or 8- to 14-μm wavelength bands. When operating in the range 3 to 5 μm, care must be taken not to include reflected sunlight in the scene.

Figure 5.23 illustrates the use of aerial thermal scanning to detect heat loss from a steam line located on an old stone arch bridge that crosses a deep gorge on the Cornell University campus. The surface of the bridge is constructed of steel-reinforced concrete. Maintenance personnel were aware of the steam leak before thermal scanning of the area, but one entire lane of the bridge was apparently hot and they were reluctant to cut through the reinforced concrete in an attempt to locate the defective section of steam line. Using various enhancements of the thermal image shown as Figure 5.23*a*, they were able to locate the heat source, which turned out to be a 6-mm-diameter hole in a 10-cm-diameter steam line. The line is insulated with asbestos and encased in a 30-cm-diameter clay tile located 60 cm below the road surface. The clay tile casing compounded the problem of precisely locating the steam leak using conventional means. That is, the casing ducted the steam a substantial distance from the leak. This caused the illusion of a general steam line failure, but close inspection of the thermal images indicated the exact site of the leak. Figure 5.23*b* shows the same bridge after correction of the steam leak.

NASA's *Thermal Infrared Multispectral Scanner (TIMS)* is a multispectral scanner that operates exclusively in the thermal infrared portion of the spectrum. It utilizes six narrow bands located between 8.2 and 12.2 μm and has an IFOV of 2.5 mrad and a total field of view of 80°. This instrument has great potential for geologic mapping because the spectral exitance of various minerals, especially silicates, is distinct in the 8- to 14-μm-wavelength region.

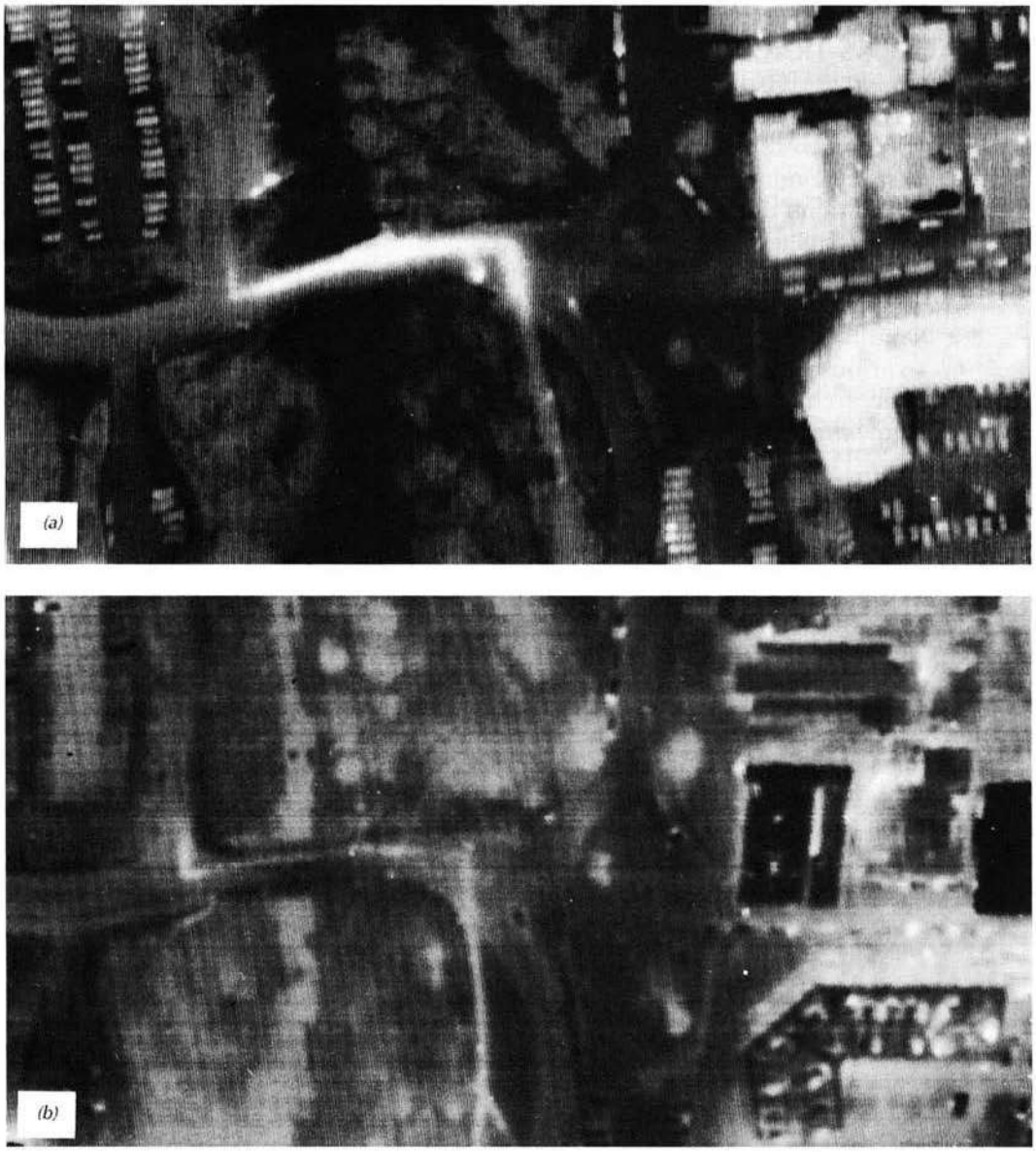

Figure 5.23 Thermal images showing steam line heat loss, Cornell University, Ithaca, NY: (*a*) prior to repair; (*b*) following repair. (Courtesy Cornell University and Daedalus Enterprises, Inc.)

5.9 GEOMETRIC CHARACTERISTICS OF ACROSS-TRACK SCANNER IMAGERY

The airborne thermal images illustrated in this discussion were all collected using across-track, or whiskbroom, scanning procedures. Not only are across-track scanners (multispectral and thermal) subject to altitude and attitude variations due to the continuous and dynamic nature of scanning, but also their images contain systematic geometric variations due to the geometry of across-track scanning. We discuss these sources of systematic and random geometric variations under separate headings below, although they occur simultaneously. Also, although we use thermal scanner images to illustrate the various geometric characteristics treated here, it should be emphasized that these characteristics hold for *all* across-track multispectral scanner images, not simply across-track thermal scanner images.

Spatial Resolution and Ground Coverage

Airborne across-track scanning systems are generally operated at altitudes in the range 300 to 12,000 m. Table 5.4 summarizes the spatial resolution and ground coverage that would result at various operating altitudes when using a system having a 90° total field of view and a 2.5-mrad IFOV. The ground resolution at nadir is calculated from Eq. 5.1 ($D = H'\beta$). The swath width W can be calculated from

$$W = 2H' \tan \theta \tag{5.14}$$

where

W = swath width
H' = flying height above terrain
θ = one-half total field of view of scanner

TABLE 5.4 Ground Resolution at Nadir and Swath Width for Various Flying Heights of an Across-Track Scanner Having a 90° Total Field of View and a 2.5-mrad IFOV

Altitude	Flying Height above Ground (m)	Ground Resolution at Nadir (m)	Swath Width (m)
Low	300	0.75	600
Medium	6,000	15	12,000
High	12,000	30	24,000

Many of the geometric distortions characterizing across-track scanner imagery can be minimized by constraining one's analysis to the near-center portion of the imaging swath. Also, as we will discuss, several of these distortions can be compensated for mathematically. However, their effect is difficult to negate completely. As a consequence, across-track images are rarely used as a tool for precision mapping. Instead, data extracted from the images are normally registered to some base map when positional accuracy is required in the interpretation process.

Tangential-Scale Distortion

Unless it is geometrically rectified, across-track imagery manifests severe scale distortions in a direction perpendicular to the flight direction. The problem arises because a scanner mirror rotating at constant angular velocity does not result in a constant speed of the scanner's IFOV over the terrain. As shown in Figure 5.24, for any increment of time, the mirror sweeps through a constant incremental arc, $\Delta\theta$. Because the mirror rotates at a constant angular velocity, $\Delta\theta$ is the same at any scan angle θ. However, as the distance between the nadir and the ground resolution cell increases, the linear ground velocity of the resolution cell increases. Hence, the ground element, ΔX, covered per unit time increases with increasing distance from the nadir. This results in image scale compression at points away from the nadir, as the ground spot covers a greater distance at its increasing ground speed. The resulting distortion is known as *tangential-scale distortion*. Note that it occurs only in the along-scan direction, perpendicular to the direction of flight. Image scale in the direction of flight is essentially constant.

Figure 5.25 schematically illustrates the effect of tangential distortion. Shown in Figure 5.25*a* is a hypothetical vertical aerial photograph taken over flat terrain containing patterns of various forms. An unrectified across-track

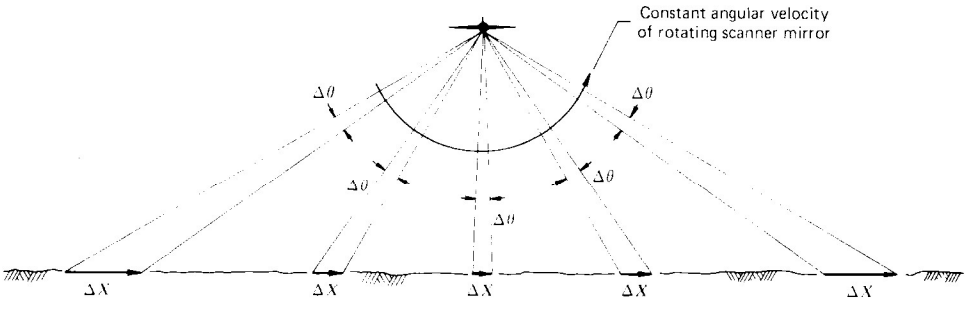

Figure 5.24 Source of tangential-scale distortion.

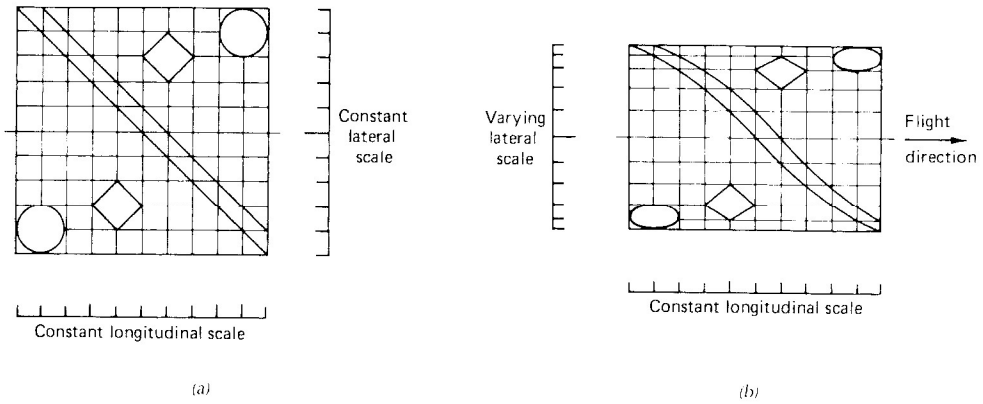

Figure 5.25 Tangential-scale distortion in unrectified across-track scanner imagery: (*a*) vertical aerial photograph; (*b*) across-track scanner imagery.

scanner image of the same area is shown in Figure 5.25*b*. Note that because of the constant longitudinal scale and varying lateral scale of the scanner imagery, objects do not maintain their proper shapes. Linear features—other than those parallel or normal to the scan lines—take on an S-shaped *sigmoid curvature*. Extreme compression of ground features characterizes the image near its edges. These effects are illustrated in Figure 5.26, which shows an aerial photograph and thermal image of the same area. The flight line for the thermal image is vertical on the page. Note that the photograph and thermal image are reproduced with the same scale along the flight line but that the scale of the thermal image is compressed in a direction perpendicular to the flight line. Two diagonal roads that are straight on the aerial photograph take on a sigmoid curvature on the thermal image. Note also the light-toned water and trees on this nighttime thermal image (similar to Figure 5.17*b*).

Figure 5.27 further illustrates tangential-scale distortion. This scanner image shows a group of cylindrical oil storage tanks. The flight line was from left to right. Note how the scale becomes compressed at the top and bottom of the image, distorting the circular shape of the tank tops. Note also that the scanner views the sides as well as the tops of features located away from the flight line.

Tangential-scale distortion normally precludes useful interpretation near the edges of unrectified across-track scanner imagery. Likewise, geometric measurements made on unrectified scanner imagery must be corrected for this distortion. Figure 5.28 shows the elements involved in computing true ground positions from measurements made on a distorted image. On unrectified imagery, y coordinates will relate directly to *angular* dimensions, not to lineal dimensions. This results in the geometric relationship depicted in the figure, where the effective focal plane of image formation is shown as a curved surface below the aircraft. In order to determine the

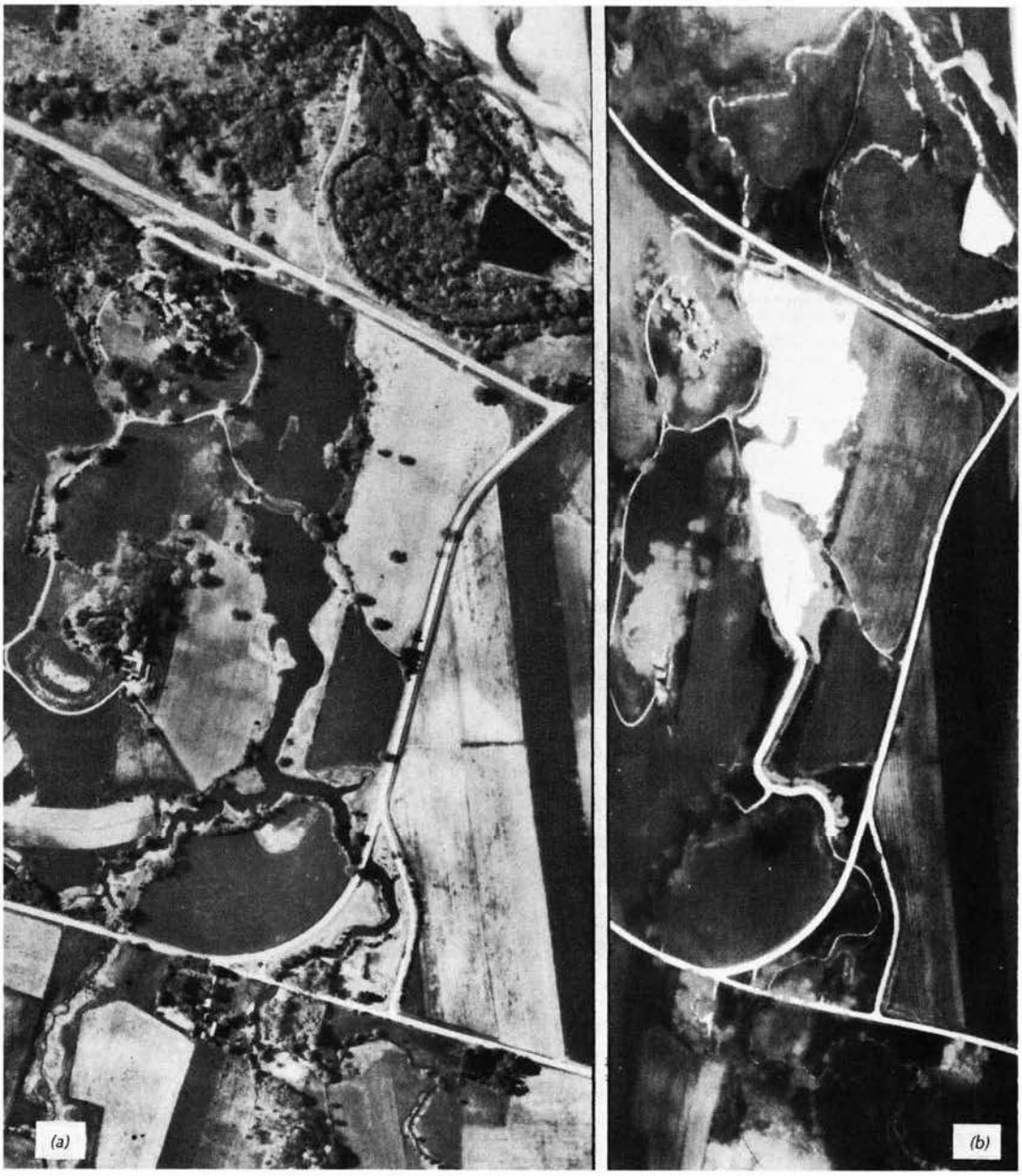

Figure 5.26 Comparison of aerial photograph and across-track thermal scanner image illustrating tangential distortion, Iowa County, WI: (*a*) panchromatic aerial photograph, 3000-m flying height; (*b*) nonrectified thermal image, 6:00 A.M., 300-m flying height. [(*a*) Courtesy USDA–ASCS. (*b*) Courtesy National Center for Atmospheric Research.]

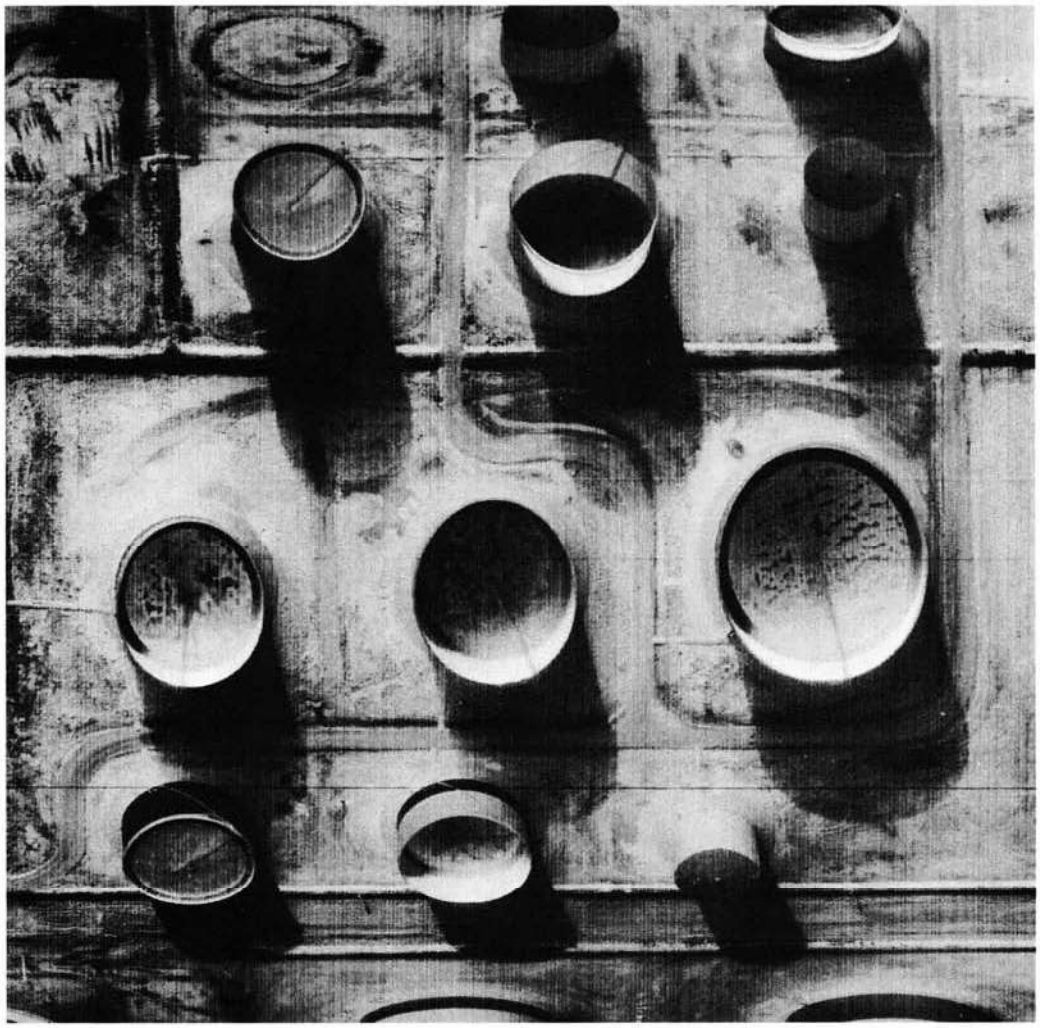

Figure 5.27 Across-track thermal scanner image illustrating tangential distortion, 100-m flying height. (Courtesy Texas Instruments, Inc.)

ground position Y_p corresponding to image point p, we must first compute θ_p from the relationship

$$\frac{y_p}{y_{\max}} = \frac{\theta_p}{\theta_{\max}}$$

Rearranging yields

$$\theta_p = \frac{y_p \theta_{\max}}{y_{\max}} \tag{5.15}$$

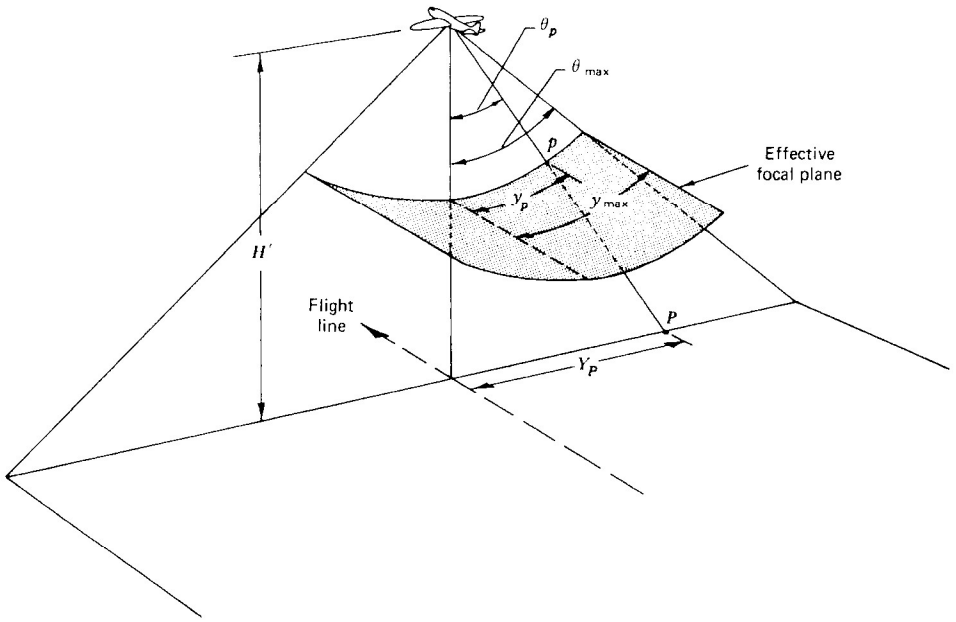

Figure 5.28 Tangential-scale distortion correction.

where

y_p = distance measured on image from nadir line to point p
y_{max} = distance from nadir line to edge of image
θ_{max} = one-half total field of view of scanner

Once θ_p has been computed, it may be trigonometrically related to ground distance Y_p by

$$Y_p = H' \tan \theta_p \tag{5.16}$$

When determining ground positions on unrectified imagery, the above process must be applied to each y coordinate measurement. Alternatively, the correction can be implemented electronically, or digitally, in the image recording process, resulting in *rectilinearized* images. In addition to permitting direct measurement of positions, rectilinearized imagery improves the ability to obtain useful interpretations in areas near the edge of images.

Resolution Cell Size Variations

Across-track scanners sense energy over ground resolution cells of continuously varying size. An increased cell size is obtained as the IFOV of a scanner moves outward from the flight nadir.

The geometric elements defining the size of the ground resolution cell are shown in Figure 5.29. At the nadir line, the ground resolution cell has a dimension of $H'\beta$. At a scan angle θ, the distance from the aircraft to the cell becomes $H'_\theta = H'$ sec θ. Hence the size of the resolution cell increases. The cell has dimensions of $(H'$ sec $\theta)\beta$ in the direction of flight and $(H'$ sec^2 $\theta)\beta$ in the direction of scanning. These are actually the *nominal* dimensions of the measurement cell. The *true* size and shape of a ground resolution cell are a function not only of β, H', and θ but also of the *response time* of a particular scanner's electronics. The response time is a measure of the time that a scanner takes to respond electronically to a change in ground reflected or emitted energy. With this added restriction, we see that optics control the resolution cell size in the direction of flight, while both optics and electronics can influence the cell size in the direction of scan. Because of system response time limitations, the resolution cell size along a scan line can be as much as three to four times that in the direction of flight.

Although it is rarely critical to know the precise degree of resolution cell size variation, it is important to realize the effect this variation has on the interpretability of the imagery at various scan angles. The scanner output at any point represents the integrated radiance from all features within the ground resolution cell. Because the cell increases in size near the edge of the image, only larger terrain features will completely fill the IFOV in these

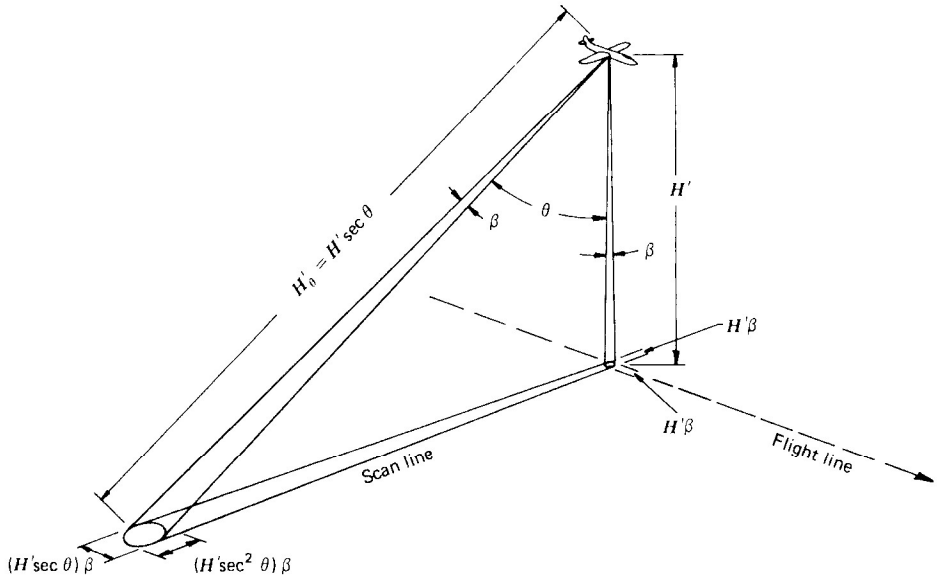

Figure 5.29 Resolution cell size variation.

areas. When objects smaller than the area viewed by the IFOV are imaged, background features also contribute to the recorded signal. This is particularly important in thermal scanning applications where accurate temperature information is required. *For an object to be registered with the proper radiant temperature, its size must be larger than the ground resolution cell.* This effect may again limit the image analysis to the central portion of the image, even after rectilinearization is performed. However, an advantage of the changing size of the ground resolution cell is that it compensates for off-nadir radiometric falloff. If the ground resolution cell area were constant, the irradiance received by the scanner would decrease as $1/H_\theta'^2$. But since the ground resolution cell area increases as $H_\theta'^2$, the irradiance falloff is precisely compensated and a consistent radiance is recorded over uniform surfaces.

One-Dimensional Relief Displacement

Figure 5.30 illustrates the nature of relief displacement characterizing across-track scanner images. Since all objects are viewed by the scanner only along "side-looking" scan lines, relief displacement occurs only in this single direction. (See also Figure 5.27.) An advantage to relief displacement is that it affords an opportunity to see a side view of objects. On the other hand, it can obscure the view of objects of interest. For example, a thermal mission might be planned to detect heat losses in steam lines in an urban setting. Tall buildings proximate to the objects of interest may completely obscure their view.

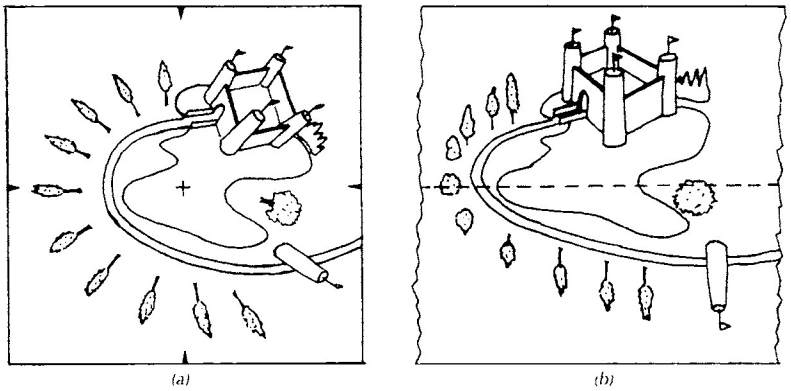

Figure 5.30 Relief displacement on a photograph versus an across-track scanner image. (*a*) In a vertical aerial photograph vertical features are displaced radially from the principal point. (*b*) In an across-track scanner image vertical features are displaced at right angles from the nadir line.

In such cases it is often necessary to cover the study area twice, in perpendicular flight directions.

Figure 5.31 is a thermal image illustrating one-dimensional relief displacement. Note that the displacement of the tops of the tall buildings is greater with increasing distance from the nadir.

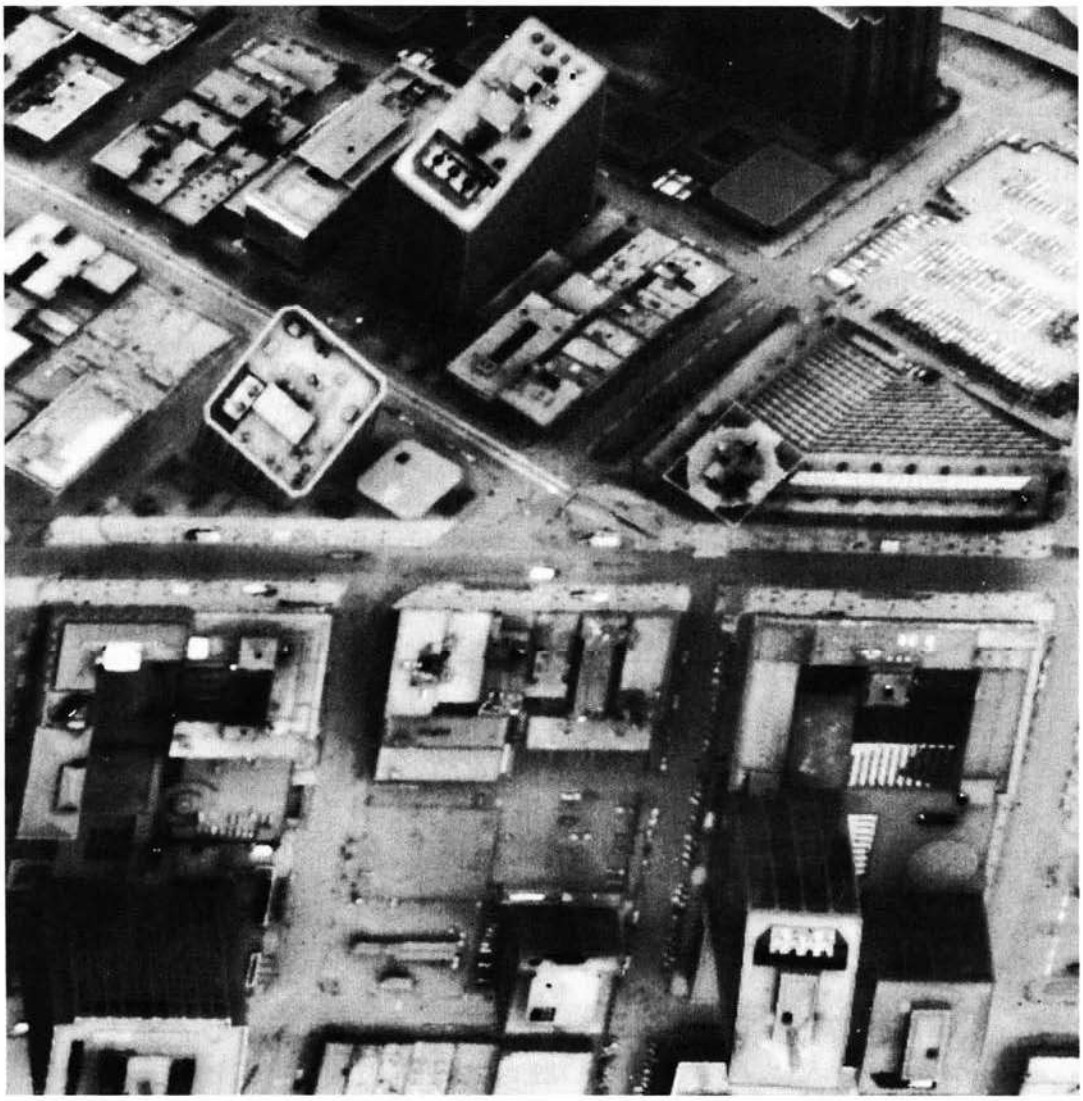

Figure 5.31 Across-track thermal scanner image illustrating one-dimensional relief displacement, San Francisco, CA, predawn, 1500-m flying height, 1 mrad IFOV. (Courtesy NASA.)

Flight Parameter Distortions

Because across-track scanner imagery is collected in a continuous fashion, it lacks the consistent relative orientation of image points found on instantaneously imaged aerial photographs. That is, across-track scanning is a dynamic continuous process rather than an intermittent sampling of discrete perspective projections as in photography. Because of this, any variations in the aircraft flight trajectory during scanning affect the relative positions of points recorded on the resulting imagery.

A variety of distortions associated with aircraft attitude (angular orientation) deviations are shown in Figure 5.32. The figure shows the effect that each type of distortion would have on the image of a square grid on the ground. This grid is shown in Figure 5.32*a*.

Figure 5.32*b* gives a sketch of an across-track scanner image acquired under constant aircraft altitude and attitude conditions. Only the tangential-scale distortion is present in this case. In Figure 5.32*c* the effect of aircraft *roll* about its flight axis is shown. Roll causes the ground grid lines to be imaged at varying times in the mirror rotation cycle. Consequently, the image takes on a wavy appearance. This effect may be negated by the process of *roll compensation*. This involves using a gyroscope to monitor aircraft roll on a line-by-line basis and appropriately advancing or retarding the start time of each scan line on the final image.

When extreme crosswind is encountered during data acquisition, the axis of the aircraft must be oriented away from the flight axis slightly to counteract the wind. This condition is called *crab* and causes a skewed image

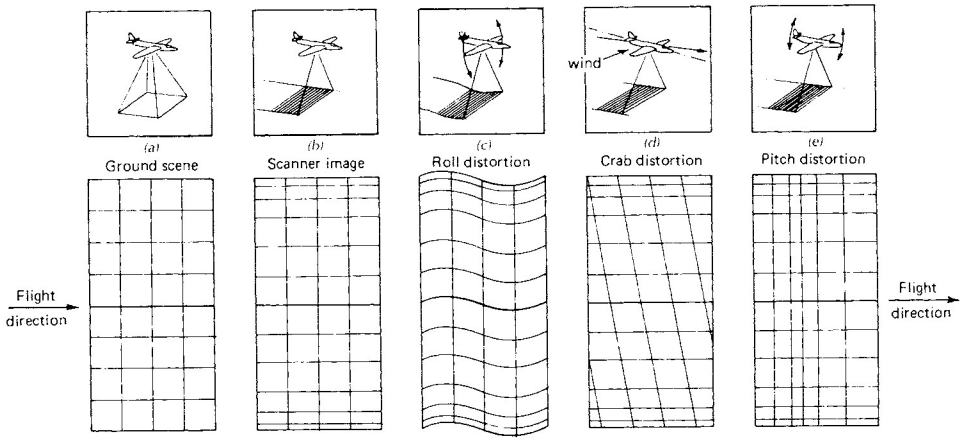

Figure 5.32 Across-track scanner imagery distortions induced by aircraft attitude deviations: (*a*) ground scene; (*b*) scanner image; (*c*) roll distortion; (*d*) crab distortion; (*e*) pitch distortion.

(Figure 5.32*d*). Crab distortion can be corrected by rotating the scanner in its ring mount during flight or by computer processing the distorted data. Most often, crab distortion is avoided by not acquiring data under high crosswind conditions.

Finally, as illustrated in Figure 5.32*e*, variations in aircraft *pitch* might distort scanner imagery. The resulting local-scale changes in the flight direction due to pitch are generally slight enough that they may be ignored in most analyses.

5.10 GEOMETRIC CHARACTERISTICS OF ALONG-TRACK SCANNER IMAGERY

The geometric characteristics of along-track scanner images are quite different from those of across-track scanner images. Along-track scanners have no scanning mirror, and there is a fixed geometric relationship among the solid-state detector elements recording each scan line. In essence, the geometry along each scan line of an along-track scanner image is similar to that of an aerial photograph. Line-to-line variation in imaging geometry is caused purely by any random variation in the altitude or attitude (angular orientation) of the aircraft along a flight line. Often, on-board inertial measurement units and GPS systems are used to measure these variations and geometrically correct the data from along-track scanners.

5.11 RADIOMETRIC CALIBRATION OF THERMAL SCANNERS

As mentioned previously, the general lack of geometric integrity of thermal scanner imagery precludes its use as a precision mapping tool. Because of this, photographic imagery is often acquired simultaneously with thermal imagery. Naturally, when nighttime thermal missions are flown, simultaneous photography is usually not feasible. In such cases, photography can be taken on the day before or after a mission. Sometimes, new photography is not needed and existing photography is used. In any case, the photography expedites object identification and study of spatial detail and affords positional accuracy. The thermal imagery is then used solely for its radiometric information content. In order to obtain accurate radiometric information from the scanner data, the scanner must be radiometrically calibrated.

There are numerous approaches to scanner calibration, each with its own degree of accuracy and efficiency. What form of calibration is used in any given circumstance is a function of not only the equipment available for data acquisition and processing but also the requirements of the application at

hand. We limit our discussion here to a general description of the two most commonly used calibration methods:

1. Internal blackbody source referencing
2. Air-to-ground correlation

As will become apparent in the following discussion, a major distinction between the two methods is that the first does not account for atmospheric effects but the second does. Other calibration methods are described by Schott (1997).

Internal Blackbody Source Referencing

Current generations of thermal scanners normally incorporate internal temperature references. These take the form of two "blackbody" radiation sources positioned so that they are viewed by the scanner mirror during each scan. The temperatures of these sources can be precisely controlled and are generally set at the "cold" and "hot" extremes of the ground scene to be monitored. Along each scan line, the scanner optics sequentially view one of the radiation standards, scan across the ground scene below the aircraft, and then view the other radiation standard. This cycle is repeated for each scan line.

Figure 5.33 illustrates the configuration of an internally calibrated scanner. The arrangement of the reference sources, or "plates," relative to the field of view of the scanner is shown in Figure 5.33*a*. The detector signal typical of one scan line is illustrated in Figure 5.33*b*. The scanner mirror sequentially looks at the cold-temperature reference plate (T_1), then sweeps the ground, and finally looks at the hot reference plate (T_2). The scanner output at the two temperature plates is recorded along with the image data. This provides a continuously updated reference by which the other scanner output values can be related to absolute radiant temperature.

The internal source referencing procedure permits acceptable calibration accuracy for many applications. Actual versus predicted temperature discrepancies of less than 0.3°C are typical for missions flown at altitudes up to 600 m under clear, dry weather conditions. However, internal calibration still does not account for atmospheric effects. As indicated earlier (Section 5.7), under many prevailing mission conditions the atmosphere can bias scanner temperature measurements by as much as 2°C.

Air-to-Ground Correlation

Atmospheric effects can be accounted for in thermal scanner calibration by using empirical or theoretical atmospheric models. Theoretical atmospheric

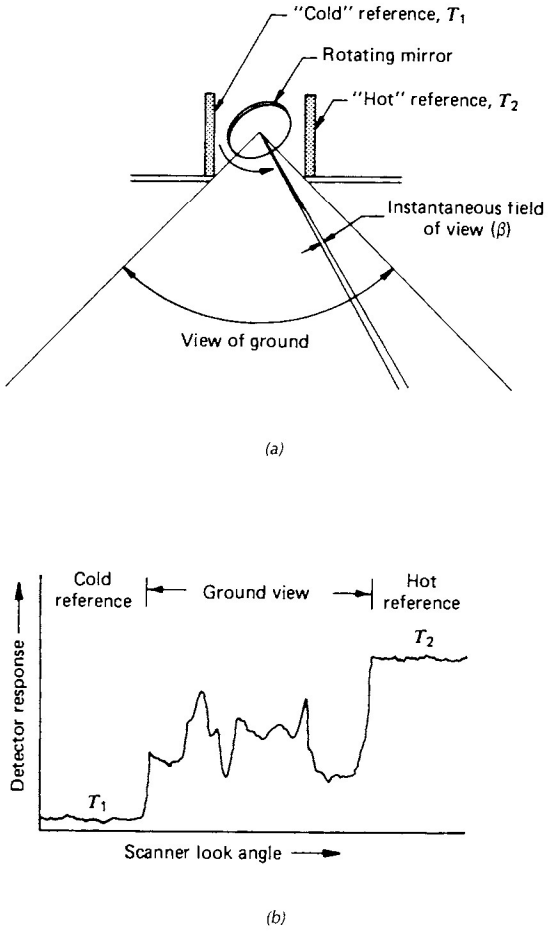

Figure 5.33 Internal blackbody source calibration: (*a*) reference plate arrangement; (*b*) typical detector output for one scan line.

models use observations of various environmental parameters (such as temperature, pressure, and CO_2 concentration) in mathematical relationships that predict the effect the atmosphere will have on the signal sensed. Because of the complexity of measuring and modeling the factors that influence atmospheric effects, these effects are normally eliminated by correlating scanner data with actual surface measurements on an empirical basis.

Air-to-ground correlation is frequently employed in calibration of thermal water quality data, such as those acquired over heated water discharges. Surface temperature measurements are taken on the ground simultaneously with the passage of the aircraft. Thermometers, thermistors, or thermal radiome-

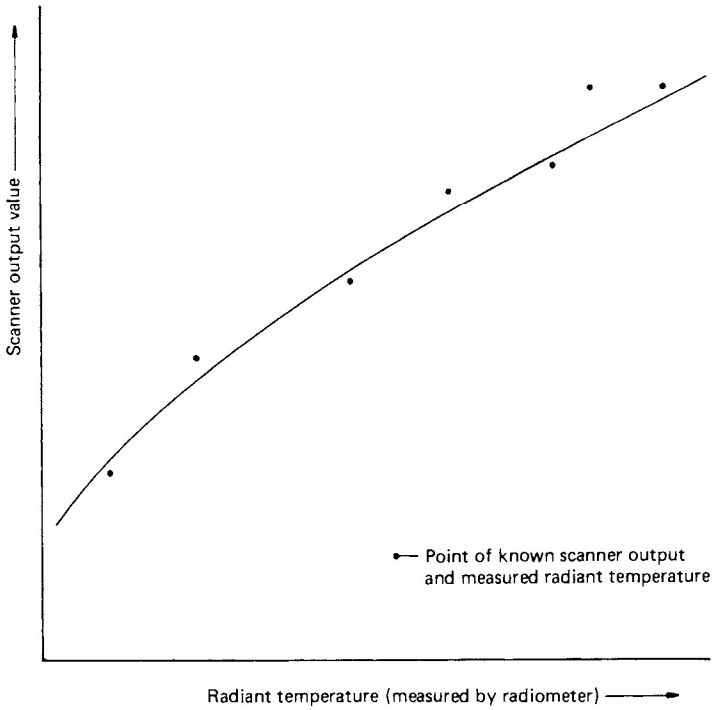

Figure 5.34 Sample calibration curve used to correlate scanner output with radiant temperature measured by radiometer.

ters operated from boats are commonly used for this purpose. Observations are typically made at points where temperatures are assumed to be constant over large areas. The corresponding scanner output value is then determined for each point of ground-based surface temperature measurement. A calibration curve is then constructed relating the scanned output values to the corresponding ground-based radiant temperature (Figure 5.34). Once the calibration relationship is defined (typically using linear regression procedures), it is used to estimate the temperature at all points on the scanner images where no ground data exist.

Figure 5.35 illustrates the type of thermal radiometer that can be used for air-to-ground correlation measurements. This particular instrument is an Everest Interscience hand-held "infrared thermometer" that operates in the 8- to 14-μm range and displays radiant temperatures on a liquid-crystal display (LCD) panel. It reads temperatures in the range from -40 to $+100$°C, with a radiometric resolution of 0.1°C and an accuracy of 0.5°C. The instrument was designed as a plant stress monitor, and its LCD panel also displays dry-bulb air temperature and differential temperature (the difference between radiant temperature and air temperature).

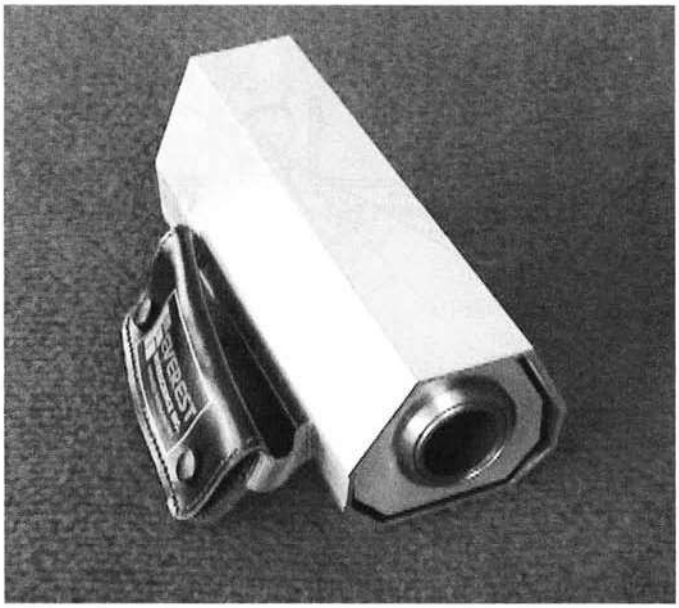

Figure 5.35 Infrared thermometer (thermal radiometer). Spot radiant temperatures are read from LCD display panel. (Courtesy Everest Interscience, Inc.)

5.12 TEMPERATURE MAPPING WITH THERMAL SCANNER DATA

In many applications of thermal scanning techniques, it is of interest to prepare "maps" of surface temperature distributions. The digital data recorded by a thermal scanner can be processed, analyzed, and displayed in a variety of ways. For example, consider scanner data for which a correlation has been developed to relate scanner output values to absolute ground temperatures. This calibration relationship can be applied to each point in the digital data set, producing a matrix of absolute temperature values.

The precise form of a calibration relationship will vary with the temperature range in question, but for the sake of the example, we assume that a linear fit of the digital data to radiant exitance is appropriate. Under this assumption, a digital number, DN, recorded by a scanner, can be expressed by

$$\mathrm{DN} = A + B\varepsilon T^4 \tag{5.17}$$

where

A, B = system response parameters determined from sensor calibration procedures described earlier
ε = emissivity at point of measurement
T = kinetic temperature at point of measurement

Once A and B are determined, kinetic temperature T for any observed digital number DN is given by

$$T = \left(\frac{\text{DN} - A}{B\varepsilon} \right)^{1/4} \tag{5.18}$$

The parameters A and B can be obtained from internal blackbody calibration, air-to-ground correlation, or any of the other calibration procedures. At a minimum, two corresponding temperature (T) and digital number (DN) values are needed to solve for the two unknowns A and B. Once parameters A and B are known, Eq. 5.18 can be used to determine the kinetic temperature for any ground point for which DN is observed *and* the emissivity is known. The calibrated data may be further processed and displayed in a number of different forms (e.g., isotherm maps, color-coded images, GIS layers).

5.13 FLIR SYSTEMS

To this point in our discussion of aerial thermography, we have emphasized scanners that view the terrain directly beneath an aircraft. *Forward-looking infrared (FLIR)* systems can be used to acquire oblique views of the terrain ahead of an aircraft. Figure 5.36 shows two images acquired by FLIR systems. Figure 5.36*a* was acquired during the daytime over a storage tank facility. Conceptually, the FLIR system used to produce this image operates on the same basic principles as an across-track line scanning system. However, the mirror for the system points forward and optically sweeps the field of view of a linear array of thermal detectors across the scene of interest. Figure 5.36*b* was acquired using a helicopter-borne FLIR system. Thermal shadows can be seen next to the parked vehicles at the left side of the image, while the

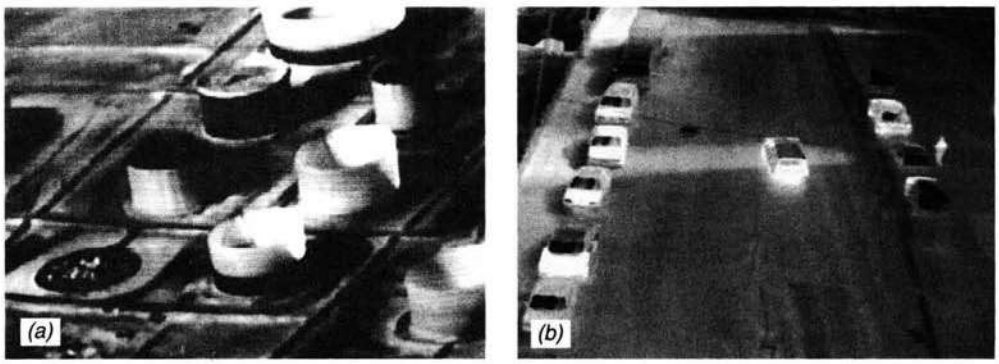

Figure 5.36 FLIR images. (*a*) Storage tank facility. Note level of liquid in each tank. (Courtesy Texas Instruments, Inc.) (*b*) City street. Note thermal shadows adjacent to parked vehicles and the image of a person on the right side of the street. (Courtesy FLIR Systems, Inc.)

moving vehicle at the center of the image does not have a thermal shadow associated with it. Note also the heat emitted from the hood of those cars that have been operated most recently and the image of a person near the right side of the image.

Modern FLIR systems are extremely portable (typically weighing less than 30 kg) and can be operated on a wide variety of fixed-wing aircraft and helicopters as well as from ground-based mobile platforms. Forward-looking imagery has been used extensively in military applications. Civilian use of FLIR is increasing in applications such as fire fighting, electrical transmission line maintenance, law enforcement activities, and nighttime vision systems for automobiles.

5.14 HYPERSPECTRAL SENSING

Hyperspectral sensors (sometimes referred to as *imaging spectrometers*) are instruments that acquire images in many, very narrow, contiguous spectral bands throughout the visible, near-IR, mid-IR, and thermal IR portions of the spectrum. (They can employ across-track or along-track scanning or two-dimensional framing arrays.) These systems typically collect 200 or more bands of data, which enables the construction of an effectively continuous reflectance (emittance in the case of thermal IR energy) spectrum for every pixel in the scene (Figure 5.37). These systems can discriminate among earth

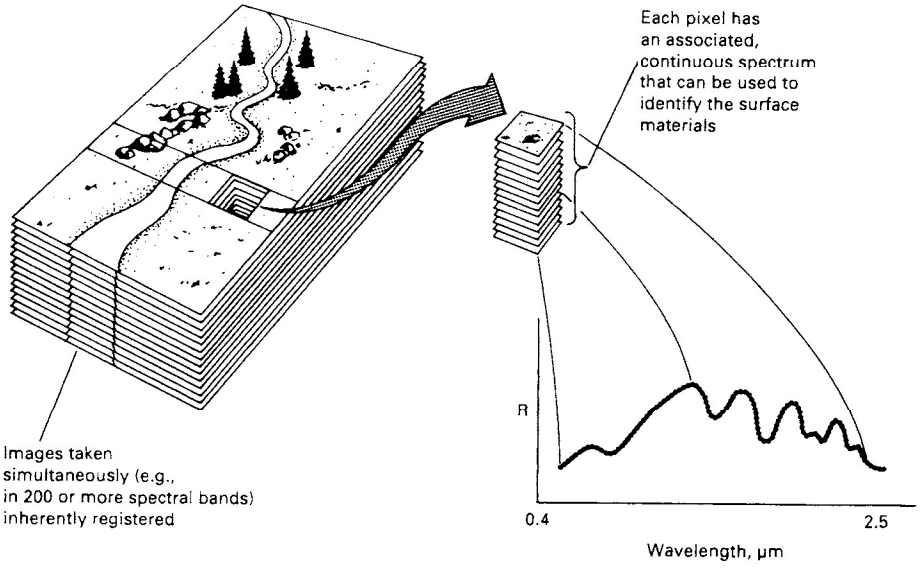

Figure 5.37 Imaging spectrometry concept. (Adapted from Vane, 1985.)